Journal of Nuclear Medicine, published on January 17, 2019 as doi:10.2967/jnumed.118.220095

Preclinical Evaluation of ^{111}In-labeled PEGylated Maytansine Nimotuzumab Drug Conjugates in EGFR-positive Cancer Models

Siddesh V. Hartimath[1], Elahe Alizadeh[1], Viswas Raja Solomon [1], Rufael Chekol[1], Wendy Bernhard[2], Wayne Hill[2], Angel Casaco Parada[3], Kris Barreto[2], Clarence Ronald Geyer[2*], Humphrey Fonge [1,4*]

[1]Department of Medical Imaging, University of Saskatchewan, College of Medicine, Saskatoon SK, Canada

[2]Department of Pathology and Laboratory Medicine, University of Saskatchewan, College of Medicine, Saskatoon SK, Canada

[3]Centre for Molecular Immunology, Havana, Cuba

[4]Department of Medical Imaging, Royal University Hospital (RUH), Saskatoon SK, Canada

Corresponding authors

*Humphrey Fonge, PhD
Dept. of Medical Imaging, room 1566
RUH Saskatoon
103 Hospital Dr,
Saskatoon, SK, S7N 0W8
humphrey.fonge@usask.ca
Tel: 306-655-3353
Fax: 306 655 1637

Clarence Ronald Geyer, PhD
Email: ron.geyer@usask.ca
Tel: 306-966-2040

Running title: Molecular Imaging of nimotuzumab ADCs

Abstract

Background: Epidermal growth factor receptor I (EGFR) is overexpressed in most cancers of epithelial origin. Antibody drug conjugates (ADCs) with PEGylated-maytansine (PEG-DM1) show promise *in vitro* and *in vivo*. However, *in vivo* biodistribution data for ADCs with PEG-DM1 have not been reported. Development of methods to understand the real-time *in vivo* behaviour of these ADCs is needed to move these compounds to the clinic.

Methods: Here we have used non-invasive μSPECT/CT imaging and *ex vivo* biodistribution to understand the *in vivo* behaviour of PEG_6-DM1 ADCs. We developed nimotuzumab ADCs conjugated to PEG_6-DM1. We generated immunoconjugates with low (nimotuzumab-PEG_6-DM1-Low) and high (nimotuzumab-PEG_6-DM1-High) drug to antibody ratios (DAR). The DAR of nimotuzumab-PEG_6-DM1-Low and nimotuzumab-PEG_6-DM1-High was 3.5 and 7.3, respectively. Quality control was performed using UV spectrophotometry, size exclusion HPLC, bioanalyzer, biolayer interferometry, and flow cytometry in EGFR-positive DLD-1 cells. These immunoconjugates were conjugated with DOTA and radiolabeled with ^{111}In. The *in vitro* binding and internalization rates of ^{111}In-nimotuzumab, ^{111}In-nimotuzumab-PEG_6-DM1-Low and ^{111}In-nimotuzumab-PEG_6-DM1-High were characterized. Furthermore, the pharmacokinetics, biodistribution and imaging characteristics were evaluated in normal and DLD-1 tumor bearing mice.

Results: Flow cytometry and biolayer interferometry showed a trend towards decreasing EGFR affinity with increasing number of PEG_6-DM1 on the antibody. Despite the lower overall cellular binding of the PEG_6-DM1 radioimmunoconjugates, internalization was higher for PEG_6-DM1 ADCs than for the non-PEGylated ADC in the following order: ^{111}In-nimotuzumab-PEG_6-DM1-High > ^{111}In-nimotuzumab-PEG_6-DM1-Low > ^{111}In-nimotuzumab. Nuclear uptake of ^{111}In-

nimotuzumab-PEG$_6$-DM1-High was 4.4-fold higher than ^{111}In-nimotuzumab. Pharmacokinetics and biodistribution showed ^{111}In-nimotuzumab-PEG$_6$-DM1-High had the slowest blood and whole body clearance rate. Uptake in DLD-1 tumors of ^{111}In-nimotuzumab was similar to ^{111}In-nimotuzumab-PEG$_6$-DM1-Low but was significantly higher than for ^{111}In-nimotuzumab-PEG$_6$-DM1-High. Tumor-to-background ratios for ^{111}In-nimotuzumab and ^{111}In-nimotuzumab-PEG$_6$-DM1-Low were higher than for ^{111}In-nimotuzumab-PEG$_6$-DM1-High.

Conclusion: The results show that conjugation of multiple PEG$_6$-DM1 reduces the affinity for EGFR *in vitro*. However, the reduced affinity is counteracted by the high internalization rate of constructs with PEG$_6$-DM1 ADCs *in vitro*. The decreased affinity resulted in low tumor uptake of ^{111}In-nimotuzumab-PEG$_6$-DM1-High with a slow overall whole body clearance rate. This data provides insights for evaluating the pharmacokinetics, normal tissue toxicity and in determining dosing rate of PEGylated ADCs.

Keywords: microSPECT/CT imaging, EGFR, ADCs, nimotuzumab, PEGylated maytansine

INTRODUCTION

The human epidermal growth factor receptor (EGFR), also known as EGFR/ErbB 1/HER 1 is a 170 kDa transmembrane cell surface glycoprotein belonging to the subfamily of type-1 tyrosine kinase receptor. Other members of this family include, ErbB-2/HER-2, ErbB-3/HER-3 and ErbB-4/HER-4 (*1*). Overexpression of EGFR is implicated in aggressive cancers of epithelial origin, including squamous cell head & neck (90 – 100%) (*2*), glioma (90 – 100%) (*3*), non-small cell lung (75 – 90%), colorectal (80 – 85%) (*4*), breast (20 – 30%) (*5*) and cervical (*6*) cancers. Anti-EGFR antibodies cetuximab (*7*), panitumumab (*8*) and nimotuzumab (*9,10*) are used to treat different EGFR positive cancers. With the exception of nimotuzumab, these antibodies are associated with significant cutaneous toxicity in 45 - 100% of patients (*11-13*). In contrast, nimotuzumab is better tolerated (*10,14*) and has low skin toxicities, because its binding affinity is 10-fold lower than other anti-EGFR antibodies ensuring transient binding to low EGFR-expressing healthy tissues such as the skin (*15*).

The efficacy of anti-EGFR antibodies is poor (*16,17*), but efficacy is improved by creating antibody drug conjugates (ADCs) (*18*). AMG-595 is an anti-EGFR ADC in phase I/II trials in which the antibody is conjugated to a cytotoxic agent maytansine (DM1) (*19*). Anti-Her2 monoclonal antibody trastuzumab conjugated to DM1 (Kadcyla®, trastuzumab-emtansine) is effective in preclinical models and in patients with Her2-positive trastuzumab- or lapatinib-resistant phenotypes, and is currently approved (*20,21*). Despite improvements in efficacy, acquired resistance through the expression of multidrug resistant gene (MDR1) by cancer cells is common with ADCs. Many cytotoxic small molecules including DM1 are substrates for MDR1 and are actively pumped out of the cell (*22-24*). ADCs developed with PEGylated DM1 (PEG-DM1) however, are more potent and are not a MDR1 substrate (*24,25*). These ADCs are also more

hydrophilic allowing conjugation of many drugs without affecting binding to antigens (*24,25*). These ADCs were several fold more potent *in vitro* and are effective against resistant cells that overexpress MDR1. Despite these promising *in vitro* results, detailed studies that investigate effects of multiple drugs on antibodies *in vivo* are not available in the literature.

Molecular imaging allows non-invasive *in vivo* assessment of the effects of drugs on the antibody. In the current study, we developed nimotuzumab ADCs using PEG_6-DM1 with low (nimotuzumab-PEG_6-DM1-Low) and high (nimotuzumab-PEG_6-DM1-High) drug to antibody ratios. To understand the effect of multiple drugs conjugated randomly to the antibody we radiolabeled nimotuzumab-PEG_6-DM1-Low, nimotuzumab-PEG_6-DM1-High and nimotuzumab with ^{111}In via a DOTA chelator and studied the *in vitro* binding characteristics and *in vivo* behavior using gamma counting techniques and single photon emission computed tomography/computed tomography (microSPECT/CT) imaging. Comparison of the *in vitro* and *in vivo* characteristics of ^{111}In-nimotuzumab-PEG_6-DM1-Low, ^{111}In-nimotuzumab-PEG_6-DM1-High and ^{111}In-nimotuzumab allowed for the real-time assessment of the effects of drugs on the antibody. The development of *in vivo* methods to understand the behavior of ADCs is important because it will enable the quantification of the receptor in real time and the understanding of the complete *in vivo* characteristics of the ADC, which is important in determining treatment regimens and normal tissue toxicity. If incorporated in clinical trials, this approach could allow for improved dosing regiments and in clinical practice could be used to stratify patients which can lead to better treatment outcomes using ADCs.

MATERIALS AND METHODS

DM1 drug was obtained from Toronto Research Chemicals and NHS-PEG_6-maleimide was purchased from Biochempeg. DLD-1 (high EGFR density/cell) and HT-29 (low EGFR density/cell) were obtained from ATCC and cultured in monolayers in RPMI-1640, DMEM/McCoy's 5A media, respectively. All media were supplemented with 10% fetal calf serum and cells were maintained in a humidified atmosphere with 5% CO_2 at 37 $^{\circ}$C. Proton magnetic resonance (^{1}HNMR) spectra were obtained on a Bruker NMR and the exact mass was determined with TOF-MS (Waters Corp.).

Synthesis of Nimotuzumab ADCs and Conjugation with *p*-SCN-Bz-DOTA

Nimotuzumab or control human antibody anti-maltose binding protein (MBP IgG) was conjugated with DM1-PEG_6-NHS. A 20 mg/mL in DMSO stock solution of the drug linker DM1-PEG_6-NHS was prepared. The conjugation reactions were optimized for pH, buffers and reaction time. In order to prepare ADCs with a low (3 – 4) or a high (7 – 8) drug to antibody ratio (DAR), a 5 – 50 mole excess equivalent of drug linker DM1-PEG_6-NHS was used to conjugate the antibodies to obtain a low (nimotuzumab-PEG_6-DM1-Low) or high (nimotuzumab-PEG_6-DM1-High) DAR. Nimotuzumab (5 mg/mL in PBS) was buffer exchanged using centrifugal filters (Amicon Ultra-4 Centrifugal Filter 10K NMCO, EMD Millipore, Burlington, MA) and allowed to react with DM1-PEG_6-NHS for 3 – 20 hours at ambient temperature. In all reactions the amount of DMSO was kept at < 3 %. The excess unconjugated drug linker was removed from the reaction mixture using a centrifugal filter and the antibody was stored in PBS. All the conjugates were passed through 0.2 μM membrane filters and aliquoted into 20 μL vials and stored at -80 ^{0}C until

further use. The DAR was then determined by UV spectrophotometry (*26*) and bioanalyzer (Agilent).

For DOTA conjugation a 25-fold excess of p-SCN-Bz-DOTA (20 mg/mL in DMSO) was incubated for 1 hour at 37°C with shaking at 500 rpm, with antibodies (5 mg/mL) buffer exchanged into 0.1 M $NaHCO_3$ (pH 8.5). Antibodies were stored and excess DOTA removed as described above. Protein concentration was determined by SmartSpec Plus spectrophotometer (Bio-Rad).

Binding Kinetics and Flow Cytometry

Binding kinetics between antibodies and target proteins were measured using ForteBio Octet RED384 (PALL Corporation). Antibodies were immobilized on anti-human FAB-CH1 sensors (18-5104, Forte Bio) according to manufacturer's instructions. The equilibrium dissociation constant (K_D) was obtained using a 1:1 model with global fitting. Data analysis and curve fitting was performed using data analysis software 7.1.0.33 (Forte Bio).

DLD-1 or HT-29 cells were treated with antibodies at ten concentrations starting with 2 μM with 3-fold serial dilutions, incubated for 30 min at room temperature followed by 15 min on ice. Cells were washed with PBS + 2% FBS and incubated with secondary antibody FITC labeled Goat $F(ab')_2$ fragment anti-human IgG (H + L) (1:50 ratio) (IM0839, Beckman Coulter) for 30 min at 4°C, then washed again. Flow data was acquired using a MACS quant VYB (Miltenyl biotech) and analyzed by FlowJoV10. 6 the EC_{50} was determined using GraphPad prism 6.

Radioligand Binding, Internalization and Immunoreactivity

Binding was determined with DLD-1 cells. A saturation radioligand binding assay was performed by incubating 0.5 million cells with increasing concentrations of

radioimmunoconjugates (0.2 – 95 nmol/L in 100 µL PBS) for 4 h at 4 °C. Non-specific binding (NSB) was determined in the presence of a 25-fold molar excess of unlabeled nimotuzumab (relative to the highest concentration of the radioimmunoconjugates). A non-linear regression analysis with one-site binding equation was used to determine K_D using GraphPad Prism 6.

Internalization of ADCs is a critical factor that determines efficacy. Internalization of the radioimmunoconjugates was performed using the Nuclei Isolation kit (NUC101, Sigma) as described earlier (*27*). The immunoreactive fraction of the radioimmunoconjugates was determined as described in Lindmo *et al.* (*28*).

Biodistribution and Pharmacokinetics

Biodistribution was performed in healthy Balb/c mice. Mice (n = 4/group) were injected with 6.5 ± 0.2 MBq of the radioimmunoconjugates and animals were sacrificed at 24 h, 72 h or 144 h post injection (p.i.). Organs were harvested and activity was measured using a gamma counter (2480 PerkinElmer). Tissue uptake was expressed as percentage of injected activity per gram (% IA/g).

The pharmacokinetics was determined in healthy Balb/c mice (n = 4/group). The animals were injected with 6.5 ± 0.0.1 MBq of the radioimmunoconjugates via a tail vein and blood was collected at various time points from a saphenous vein in heparinized capillary tubes. Radioactivity in blood activity was expressed as (% IA/mL). Relevant pharmacokinetic parameters were determined using an exponential decay curve fitting from sigma plot using GraphPad Prism 6.

MicroSPECT/CT Imaging

DLD-1 tumor bearing mice were injected via tail vein with 12 – 15 MBq of radioimmunoconjugates. The mice were anesthetized using isoflurane/oxygen (5 % induction, and 2 % maintenance), SPECT/CT images were acquired at 24, 48, 72, 96, 120, 144 and 168 h.p.i. using the Vector^{4}CT scanner (MILabs B.V.). A 30-min full body SPECT scan was acquired in a list-mode data format with a high-energy ultra-high-resolution mouse pinhole collimator (HE-U H-1.0 mm) followed by full body CT scan with tube setting 50kV and 480 μA. Body temperature, heart rate and respiration of animals were continuously monitored.

Image reconstructions were carried out with a pixel-based order-subset expectation maximization (POS-EM) algorithm that included resolution recovery and compensation for distance-dependent pinhole sensitivity. For the SPECT images, we used 16 subsets and 10 iterations (160 ML-EM equivalent) image reconstruction with an isotropic 0.8 mm-voxel grid. CT was reconstructed using Hann projection with a filter of a 150-mm voxel grid to generate a 3D CT image. Reconstructed SPECT images are quantified to correct for attenuation, using the CT image as an attenuation map for non-uniform attenuation correction. The registered CT and quantified SPECT images were analyzed using PMOD 3.8 software (PMOD). Region-of-interest (ROI) was manually drawn around tumor, heart, liver, muscle, kidneys and bladder, and uptake was expressed as mean percentage injected activity per volume (% IA/cc ± standard deviation). At the end of imaging (168 h p.i.), mice were euthanized followed by biodistribution studies. Uptake in all organs was expressed as % IA/g

Statistical Analysis

All data was expressed as the mean ± SD or SEM of at least 3 independent experiments. Statistical significance between groups was assessed using a two-tailed Student's *t*-test or analysis of variance (ANOVA) with Bonferoni post hoc test. Graphs were prepared and analyzed using GraphPad Prism (version 6; GraphPad).

RESULTS

Characterization of Immunoconjugates

We developed nimotuzumab ADCs nimotuzumab-PEG_6-DM1-Low and nimotuzumab-PEG_6-DM1-High with low (~ 3.5) and high (~ 7.3) DARs (Supplemental Fig. 1 and 2). Nimotuzumab, nimotuzumab-PEG_6-DM1-Low and nimotuzumab-PEG_6-DM1-High were conjugated to DOTA to allow radiolabeling with ^{111}In (Supplemental Fig. 3). HPLC showed the conjugates were > 98% pure with < 1% aggregates or degradation (Supplemental Fig. 4). Bioanalyzer showed the purity and size of nimotuzumab, nimotuzumab-PEG_6-DM1-Low, nimotuzumab-PEG_6-DM1-High and their respective DOTA conjugated immunoconjugates (Supplemental Fig. 5A)

The effect of DOTA conjugation on the dissociation constant (K_D) to recombinant EGFR was studied using biolayer interferometry (Supplemental Fig. 5B, Table 1). The K_D of DOTA-nimotuzumab was not significantly different ($p = 0.09$) from nimotuzumab. However, the K_Ds of DOTA-nimotuzumab-PEG_6-DM1-Low and DOTA-nimotuzumab-PEG_6-DM1-High were respectively 5.7-fold ($p < 0.05$) and 21-fold ($p = 0.05$) higher than for nimotuzumab (Table 1).

Binding of the immunoconjugates to EGFR-positive DLD-1 (high EGFR expression) and HT-29 (low EGFR expression) cells was studied by flow cytometry (Fig. 1). The EC_{50} of

nimotuzumab was 3.4-fold lower than DOTA-nimotuzumab (11.6 ± 2.6 nM vs 39.2 ± 5.6 nM; $p = 0.79$). The EC_{50} of DOTA-nimotuzumab-PEG_6-DM1-Low (76.5 ± 4.68 nM) and DOTA-nimotuzumab-PEG_6-DM1-High (90.7 ± 6.35 nM) was respectively, 2-fold ($p < 0.05$) and 2.3-fold ($p < 0.05$) higher than DOTA-nimotuzumab.

Radiolabeling and Stability of Radioimmunoconjugates

To optimize the labeling with ^{111}In, different radiolabeling conditions were studied: time (60 or 90 min), temperature (RT or 37 °C), pH (4.5 – 6) and specific activity (0.1 – 1.5 MBq/μg). The best radiochemical yield was obtained using 0.5 MBq/μg, pH 5.0 at room temperature after 90 min incubation. Under these conditions, the average radiochemical yield for all the tracers was 65 ± 3% with a radiochemical purity > 98% (Supplemental Fig. 4).

The radioimmunoconjugates were stable in human plasma and PBS following incubation at 37 ºC for 5 days (Supplemental Fig. 6A). Dissociation of ^{111}In from the complex was studied in challenge experiments using several-fold excess of other metal ions: Ca^{2+}, Mg^{2+}, Fe^{2+} and Zn^{2+}. All radioimmunoconjugates showed dissociation in the presence of 1 M Fe^{2+} ions, with 50% released from the DOTA complex (Supplemental Fig. 6B – D).

Radioligand Binding and Immunoreactivity

To verify if radiolabeling affected the binding of the radioimmunoconjugates, a saturation binding assay was performed using EGFR positive DLD-1 cells (Fig. 2). The estimated K_D of ^{111}In-nimotuzumab, ^{111}In-nimotuzumab-PEG_6-DM1-Low and ^{111}In-nimotuzumab-PEG_6-DM1-High was 25 ± 4.3 nM, 167 ± 6.3 nM, and 303 ± 8.6 nM, respectively. The values for ^{111}In-

nimotuzumab-PEG$_6$-DM1-Low and ^{111}In-nimotuzumab-PEG$_6$-DM1-High were respectively, 6-fold ($p < 0.05$) and 12-fold ($p < 0.05$) higher than for ^{111}In-nimotuzumab.

The immunoreactive fraction of ^{111}In-nimotuzumab, ^{111}In-nimotuzumab-PEG$_6$-DM1-Low and ^{111}In-nimotuzumab-PEG$_6$-DM1-High was 0.83, 0.70 and 0.58, respectively (Supplemental Fig. 7). There was a decrease in the immunoreactive fraction of the antibody with increasing number of drugs on the antibody. The immunoreactive fraction of ^{111}In-nimotuzumab-PEG$_6$-DM1-High was significantly lower ($p < 0.05$) than ^{111}In-nimotuzumab.

Internalization of Radioimmunoconjugates

Internalization of all radioimmunoconjugates increased over time (Fig. 3A). The highest internalization rate was observed at 48 h post incubation with ^{111}In-nimotuzumab-PEG$_6$-DM1-High (41%) > ^{111}In-nimotuzumab-PEG$_6$-DM1-Low (40%) > ^{111}In-nimotuzumab (37%). The amount of membrane bound immunoconjugate was highest for ^{111}In-nimotuzumab followed by ^{111}In-nimotuzumab-PEG$_6$-DM1-Low and ^{111}In-nimotuzumab-PEG$_6$-DM1-high (Fig. 3B), which was in line with the lowest K_D for ^{111}In-nimotuzumab. Cytoplasmic bound tracer increased in the order ^{111}In-nimotuzumab > ^{111}In-nimotuzumab-PEG$_6$-DM1-Low > ^{111}In-nimotuzumab-PEG$_6$-DM1-High (Fig. 3C), with a statistically higher ($p < 0.05$) cytoplasmic uptake of ^{111}In-nimotuzumab compared with ^{111}In-nimotuzumab-PEG$_6$-DM1-Low and ^{111}In-nimotuzumab-PEG$_6$-DM1-High. Interestingly, the nuclear bound fraction was similar for ^{111}In-nimotuzumab-PEG$_6$-DM1-Low and ^{111}In-nimotuzumab-PEG$_6$-DM1-High and was significantly ($p < 0.05$) higher than ^{111}In-nimotuzumab (Fig. 3D). Highest nuclear uptake was observed at 4 h for the drug conjugates (^{111}In-nimotuzumab-PEG$_6$-DM1-Low (48.4%) vs ^{111}In-nimotuzumab-PEG$_6$-DM1-High (53.1%)) and decreased thereafter. There was negligible uptake of the control antibody ^{111}In-ctrl-IgG and

drug conjugates of the control antibody ^{111}In-ctrl-IgG-PEG$_6$-DM1-Low and ^{111}In-ctrl-IgG-PEG$_6$-DM1-High (Fig. 3A).

Biodistribution and Pharmacokinetics

Normal tissue biodistribution of ^{111}In-nimotuzumab, ^{111}In-nimotuzumab-PEG$_6$-DM1-Low and ^{111}In-nimotuzumab-PEG$_6$-DM1-High was studied in healthy Balb/C mice (n = 4/ tracer and time point) at 24, 72 and 144 h p.i. (Fig. 4A – C). Whole body clearance of the tracer was slowest for ^{111}In-nimotuzumab-PEG$_6$-DM1-High. Clearance from major organs was in the order ^{111}In-nimotuzumab-PEG$_6$-DM1-High < ^{111}In-nimotuzumab-PEG$_6$-DM1-Low < ^{111}In-nimotuzumab. The clearance was largely determined by the half-life in blood with ^{111}In-nimotuzumab-PEG$_6$-DM1-High showing the highest blood retention at all time points. At 144 h p.i. ^{111}In-nimotuzumab was almost completely cleared from all organs except for the liver (2.91 ± 0.37 %IA/g) and kidney (2.41 ± 0.23 %IA/g). There was a higher residual bone uptake of the ^{111}In-nimotuzumab-PEG$_6$-DM1-High and ^{111}In-nimotuzumab-PEG$_6$-DM1-Low compared to ^{111}In-nimotuzumab with the highest uptake observed at the 144 h. The presence of the PEG$_6$-DM1 led to significantly higher renal clearance of the ^{111}In-nimotuzumab-PEG$_6$-DM1-Low and ^{111}In-nimotuzumab-PEG$_6$-DM1-High compared with the ^{111}In-nimotuzumab immunoconjugate.

Pharmacokinetics of all radioimmunoconjugates was studied in normal Balb/C mice (Fig. 5). All tracers exhibited a bi-phasic half-life with a fast (distribution) $t_{1/2\alpha}$ and a slow clearance $t_{1/2\beta}$ (Table 2). There was a trend towards longer circulation with the number of drugs (PEG$_6$-DM1) on the antibody with the ^{111}In-nimotuzumab-PEG$_6$-DM1-High exhibiting the longest circulation time. However, with the exception of area under the curve (AUC), which was longest ($p < 0.05$) for

^{111}In-nimotuzumab-PEG$_6$-DM1-High. No significant differences were found for all of the pharmacokinetic parameters studied.

µSPECT Imaging and Biodistribution in Mouse Xenograft

µSPECT imaging was performed in athymic CD-1 nude mice bearing DLD-1 xenograft at different time points (Fig. 6A). Unequivocal delineation of xenograft was seen with nimotuzumab radioimmunoconjugates at 48 h.p.i and remained persistent at 168 h.p.i. ^{111}In-ctrl-IgG had negligible tumor uptake. As with all immunoglobulins intense liver uptake was visible. Apart from tumor and liver, we also noticed high accumulation in auxiliary lymph nodes in all the groups. Kidneys and bladder were also visible even after 24 h.p.i., but decreased at later time points.

Time activity curves (TACs) were generated for tumor (Fig. 6B). No significant difference in tumor uptake was seen between ^{111}In-nimotuzumab and ^{111}In-nimotuzumab-PEG$_6$-DM1-Low at any time point. However, tumor uptake was significantly higher for ^{111}In-nimotuzumab compared to ^{111}In-nimotuzumab-PEG$_6$-DM1-High at later time points (144 h: $p < 0.0001$; and 168 h: $p < 0.001$). Tumor uptake of ^{111}In-nimotuzumab-PEG$_6$-DM1-Low was also higher (48 h: $p < 0.001$; 72 h: $p <$ 0,001; 144: $p < 0.0001$; and 168 h: $p < 0.01$) than ^{111}In-nimotuzumab-PEG$_6$-DM1-High at all time points except at 24 h ($p > 0.05$) when this difference was not statistically significant. Peak tumor uptake on µSPECT was observed at 72 h and was 11.8 ± 0.22 %IA/cc, 12.63 ± 1.08 %IA/cc and 9.83 ± 1.13 %IA/cc for ^{111}In-nimotuzumab, ^{111}In-nimotuzumab-PEG$_6$-DM1-Low and ^{111}In-nimotuzumab-PEG$_6$-DM1-High, respectively.

There were no differences in liver uptake of ^{111}In-nimotuzumab compared with ^{111}In-nimotuzumab-PEG$_6$-DM1-Low (Fig. 6C). However, liver uptake of ^{111}In-nimotuzumab-PEG$_6$-DM1-High was slightly higher than ^{111}In-nimotuzumab and ^{111}In-nimotuzumab-PEG$_6$-DM1-Low;

this difference was significant only at later time points. Differences in tumor-to-liver ratios were mostly not statistically significant (Supplemental Fig. 8). On the other hand, tumor-to-muscle ratios were higher for ^{111}In-nimotuzumab and ^{111}In-nimotuzumab-PEG$_6$-DM1-Low compared with ^{111}In-nimotuzumab-PEG$_6$-DM1-High at 72, 144 and 168 h time points (Supplemental Fig. 8). Biodistribution at 168 h p.i. confirmed the μSPECT observations (Fig. 7). Higher spleen and liver uptake was seen with ^{111}In-nimotuzumab-PEG$_6$-DM1-High.

DISCUSSION

Several factors account for why antibodies have not lived up to expectations as immunotherapeutics. *De novo* and acquired resistance to immunotherapeutics is a common phenomenon in oncology. Cancer cells develop intrinsic resistance by overexpression of alternate growth factors and their receptors. EGFR overexpression for example, is a widely accepted mechanism of acquired resistance to epidermal growth factor receptor II (Her2) targeted treatments (*29*). Overexpression of MDR1 is a widely accepted mechanism of *de novo* resistance by cancer cells to small molecule drugs (*22-24*). DM1 has been one of the drugs of choice for many ADCs. Once internalized the DM1 is cleaved from the antibody in lysosomes and becomes toxic to the cell. However, there is strong evidence that DM1 just like many other small molecule therapeutics is a substrate for MDR1. This effect has been seen with Her2 targeted Kadcyla (trastuzumab-DM1) as well as AMG-595 (anti-EGFR-DM1) (*22,23*). However, PEG$_6$-DM1 as proposed in this study, is not a substrate of MDR1 (*24,25*).

An optimum DAR is needed to preserve biological characteristics of the antibody. Zhao *et al.* showed that a DAR of 9 using PEG linkers yielded ADCs that were more cytotoxic *in vitro* than the routinely used DAR of 3 – 4 (*25*). In this study, we developed nimotuzumab-PEG$_6$-DM1-

Low and nimotuzumab-PEG$_6$-DM1-High ADCs with DARs of 3.5 and 7.3, respectively. We used *in vitro* assays, non-invasive real-time microSPECT/CT imaging and *ex vivo* biodistribution to characterize the behaviour of PEGylated nimotuzumab ADC immunoconjugates by radiolabeling the nimotuzumab-PEG$_6$-DM1-Low/High with ^{111}In.

We showed by biolayer interferometry that in comparison with nimotuzumab, the binding of nimotuzumab-PEG$_6$-DM1-Low (1.94 nM) and nimotuzumab-PEG$_6$-DM1-High (3.75 nM) to recombinant EGFR was lower. The chelator to antibody ratio following the conjugation of DOTA was 2.8 ± 0.2 for nimotuzumab, nimotuzumab-PEG$_6$-DM1-Low and nimotuzumab-PEG$_6$-DM1-High. Size exclusion chromatography and bioanalyzer showed that DOTA-nimotuzumab, DOTA-nimotuzumab-PEG$_6$-DM1-Low and DOTA-nimotuzumab-PEG$_6$-DM1-High were exclusively monomeric species. Conjugation of DOTA led to an increase in K_D compared with the antibody without DOTA chelator. Flow cytometry showed that binding to cells was altered by conjugation reactions. Saturated radioligand binding experiments show that radiolabeling did not alter the binding of the radioimmunoconjugates to EGFR positive cells.

The potency of ADCs is dependent on lysosomal processing and release of cleaved lysine-SMCC-DM1, which is then toxic to cancer cells (*30*). Kovtun *et al.* showed that PEG$_4$-Mal-DM1 conjugated to an anti-EpCAM antibody followed the same lysosomal proteolytic pathway as DM1-conjugated ADCs. Anti-EpCAM-PEG$_4$-DM1 was processed by EpCAM positive cells resulting in a polar lysine-PEG$_4$-DM1 metabolite which was equally cytotoxic to cells (*24*). The higher internalization rate of ^{111}In-nimotuzumab-PEG$_6$-DM1-High probably explains the higher *in vitro* potency of PEG-DM1 immunoconjugates with high DAR. EGFR is a highly internalizing antigen and it has been shown that binding of anti-EGFR antibodies to EGFR enhances internalization of the antigen-antibody complex (*31*). Whether the ADCs internalize better than the antibody is very

much a matter of debate and depends on the antibody-antigen complex as well as other adapter molecules. Some authors have shown internalization rate for ADCs to be higher than the unconjugated antibody while others have shown the opposite or similar rates of internalization (*32*). Smith *et al*. (*33*) showed that anti-melanotransferrin antibody drug conjugate in which the antibody (L49) was conjugated to auristatin cytotoxin internalized better than the unconjugated antibody. Similarly, Law *et al. (34)* compared the rates of internalization of anti-CD20 rituximab, rituximab conjugated to monomethyl auristatin E (rituximab-vcMMAE) or doxorubicin (rituzumab-vcDox) in CD20 positive cells. The rate of internalization was highest for rituzumab-vcDox followed by rituximab-vcMMAE. Unconjugated rituximab had very low internalization rate in these CD20 positive cells. As was shown for cetuximab-EGFR complex (*35*), it is possible that the binding of nimotuzumab ADCs follow similar clathrin-independent (macropinocytosis) pathway which results in higher internalization rates, and hence, enhanced processing of the ADCs. Overall total binding decreased with increasing number of PEG_6-DM1 on antibody. This was consistent with the higher K_D of immunoconjugates with drug relative to immunoconjugates alone. Despite lower overall cellular binding, internalization increased with increasing number of drugs on the antibody. Particularly, at 4 h post treatment nuclei uptake of ^{111}In-nimotuzumab-PEG_6-DM1-High was similar to ^{111}In-nimotuzumab-PEG_6-DM1-Low but was 4.4-fold higher than for ^{111}In-nimotuzumab. Higher nuclear uptake leads to increased chance of double DNA strand break and hence apoptotic cell death.

Pharmacokinetics and biodistribution in normal mice showed a longer distribution half-life with increasing number of PEG_6-DM1 on the antibody with ^{111}In-nimotuzumab-PEG_6-DM1-High showing the longest $t_{1/2\beta}$. These results correlate with previous studies which showed that PEGylation increases the half-life of peptides and macromolecules (*36*). Other studies have shown

that the higher the number of drugs (non-PEGylated) on the antibody the faster the clearance of the immunoconjugate from circulation (*37,38*). The long plasma half-life of ^{111}In-nimotuzumab-PEG$_6$-DM1-High resulted in slow overall clearance of the immunoconjugate from most major organs at 168 h p.i. while ^{111}In-nimotuzumab was completely cleared at this time. This longer half-life has implications for dosing of the PEGylated ADCs. Biodistribution in mice bearing DLD-1 xenograft showed a trend towards decreasing tumor uptake with the number of PEG$_6$-DM1 on the antibody. Tumor uptake of ^{111}In-nimotuzumab was similar to ^{111}In-nimotuzumab-PEG$_6$-DM1-Low. However, tumor uptake of ^{111}In-nimotuzumab was higher than ^{111}In-nimotuzumab-PEG$_6$-DM1-High, implying that the lower EGFR binding of ^{111}In-nimotuzumab-PEG$_6$-DM1-High as evident by the higher K_D resulted in decreased EGFR binding/uptake in the DLD-1 xenograft *in vivo*. μSPECT imaging further confirmed the significantly lower tumor uptake of ^{111}In-nimotuzumab-PEG$_6$-DM1-High at 48, 72, 144 and 168 h p.i.. Tumor-to-muscle ratios of ^{111}In-nimotuzumab-PEG$_6$-DM1-High were equally lower than for ^{111}In-nimotuzumab and ^{111}In-nimotuzumab-PEG$_6$-DM1-Low at most time points.

In this work the ADCs have been radiolabeled at one or more of the lysine residues on the antibody. While this approach has tremendous potential in the understanding of the *in vivo* behavior of the ADCs, it does not provide sufficient insights on the rate of lysosomal cleavage/processing of the drug (PEG$_6$-DM1) from the antibody which is partly responsible for the efficacy of the ADC.

CONCLUSION

In this work, using PEG$_6$-DM1, we developed nimotuzumab ADCs with low (nimotuzumab-PEG$_6$-DM1-Low: DAR 3.5) and high (nimotuzumab-PEG$_6$-DM1-High: DAR 7.3)

DAR. ^{111}In-nimotuzumab, ^{111}In-nimotuzumab-PEG$_6$-DM1-Low and ^{111}In-nimotuzumab-PEG$_6$-DM1-High were developed to understand the effect of drug conjugation on the antibody using μSPECT and *ex vivo* biodistribution. *In vitro* characterization of immunoconjugates showed significantly decreased affinity for EGFR with increasing number of PEG$_6$-DM1 on the antibody. Interestingly, ADCs with higher DAR had higher internalization rates, which may account for the higher potency seen with these ADCs. Although there was no differences in tumor uptake between ^{111}In-nimotuzumab and ^{111}In-nimotuzumab-PEG$_6$-DM1-Low, tumor uptake was significantly lower for ^{111}In-nimotuzumab-PEG$_6$-DM1-High. This result implies that at same dosing rate nimotuzumab-PEG$_6$-DM1-High could be less effective *in vivo*. This imaging data confirms our recent findings that nimotuzumab-PEG$_6$-DM1-Low was more potent than nimotuzumab-PEG$_6$-DM1-High in DLD-1 tumors. Administration of 15 mg/Kg nimotuzumab-PEG$_6$-DM1-Low led to complete remission in 4/6 mice while same dose resulted in remission in 2/6 mice in nimotuzumab-PEG$_6$-DM1-High (unpublished data). Non-invasive μSPECT imaging allowed for the understanding of the *in vivo* behavior of the ADCs and can be used to determine dosing.

Acknowledgement and Funding

This study was funded by a grants from the Canadian Breast Cancer Research (No. 300030) and Saskatchewan Health Research Foundation (No. 3554). Nimotuzumab was provided by the Center for Molecular Immunology (Havana, Cuba) under the terms of a research collaboration agreement. The authors wish to acknowledge the contributions of all other members of the Geyer and Fonge Labs.

CONFLICT OF INTEREST

All authors declare they have no conflicts of interest.

Compliance with Animal Ethics

All applicable international, national, and/or institutional guidelines for the care and use of animals were followed – University of Saskatchewan animal protocol # 20170084

REFERENCES

1. Robinson DR, Wu YM, Lin SF. The protein tyrosine kinase family of the human genome. *Oncogene.* 2000;19:5548-5557.

2. Chung CH, Ely K, McGavran L, et al. Increased epidermal growth factor receptor gene copy number is associated with poor prognosis in head and neck squamous cell carcinomas. *J Clin Oncol.* 2006;24:4170-4176.

3. Alshenawy HA. Immunohistochemical expression of epidermal growth factor receptor, E-cadherin, and matrix metalloproteinase-9 in ovarian epithelial cancer and relation to patient deaths. *Ann Diagn Pathol.*2010;14:387-395.

4. Cunningham D, Humblet Y, Siena S, et al. Cetuximab monotherapy and cetuximab plus irinotecan in irinotecan-refractory metastatic colorectal cancer. *N Engl J Med.* 2004;351:337-345.

5. Giltnane JM, Ryden L, Cregger M, Bendahl PO, Jirstrom K, Rimm DL. Quantitative measurement of epidermal growth factor receptor is a negative predictive factor for tamoxifen response in hormone receptor positive premenopausal breast cancer. *J Clin Oncol.* 2007;25:3007-3014.

6. Bellone S, Frera G, Landolfi G, et al. Overexpression of epidermal growth factor type-1 receptor (EGF-R1) in cervical cancer: implications for cetuximab-mediated therapy in recurrent/metastatic disease. *Gynecol Oncol.* 2007;106:513-520.

7. Bonner JA, Harari PM, Giralt J, et al. Radiotherapy plus cetuximab for squamous-cell carcinoma of the head and neck. *N Engl J Med.* 2006;354:567-578.

8. Addeo R, Caraglia M, Cerbone D, et al. Panitumumab: a new frontier of target therapy for the treatment of metastatic colorectal cancer. *Expert Rev Anticancer Ther.* 2010;10:499-505.

9. Ramos TC, Figueredo J, Catala M, et al. Treatment of high-grade glioma patients with the humanized anti-epidermal growth factor receptor (EGFR) antibody h-R3: report from a phase I/II trial. *Cancer Biol Ther.* 2006;5:375-379.

10. Crombet T, Osorio M, Cruz T, et al. Use of the humanized anti-epidermal growth factor receptor monoclonal antibody h-R3 in combination with radiotherapy in the treatment of locally advanced head and neck cancer patients. *J Clin Oncol.* 2004;22:1646-1654.

11. Molinari E, De Quatrebarbes J, Andre T, Aractingi S. Cetuximab-induced acne. *Dermatology.* 2005;211:330-333.

12. Keating GM. Panitumumab: a review of its use in metastatic colorectal cancer. *Drugs.* 2010;70:1059-1078.

13. Lacouture ME. Mechanisms of cutaneous toxicities to EGFR inhibitors. *Nat Rev Cancer.* 2006;6:803-812.

14. Rojo F, Gracias E, Villena N, et al. Pharmacodynamic trial of nimotuzumab in unresectable squamous cell carcinoma of the head and neck: a SENDO Foundation study. *Clin Cancer Res.* 2010;16:2474-2482.

15. Garrido G, Tikhomirov IA, Rabasa A, et al. Bivalent binding by intermediate affinity of nimotuzumab: a contribution to explain antibody clinical profile. *Cancer Biol Ther.* 2011;11:373-382.

16. De Roock W, De Vriendt V, Normanno N, Ciardiello F, Tejpar S. KRAS, BRAF, PIK3CA, and PTEN mutations: implications for targeted therapies in metastatic colorectal cancer. *Lancet Oncol.* 2011;12:594-603.

17. De Roock W, Jonker DJ, Di Nicolantonio F, et al. Association of KRAS p.G13D mutation with outcome in patients with chemotherapy-refractory metastatic colorectal cancer treated with cetuximab. *JAMA.* 2010;304:1812-1820.

18. Ojima I. Guided molecular missiles for tumor-targeting chemotherapy--case studies using the second-generation taxoids as warheads. *Acc Chem Res.* 2008;41:108-119.

19. Hamblett KJ, Kozlosky CJ, Siu S, et al. AMG 595, an Anti-EGFRvIII antibody-drug conjugate, Induces potent antitumor activity against EGFRvIII-expressing glioblastoma. *Mol Cancer Ther.* 2015;14:1614-1624.

20. LoRusso PM, Weiss D, Guardino E, Girish S, Sliwkowski MX. Trastuzumab emtansine: a unique antibody-drug conjugate in development for human epidermal growth factor receptor 2-positive cancer. *Clin Cancer Res.* 2011;17:6437-6447.

21. Verma S, Miles D, Gianni L, et al. Trastuzumab emtansine for HER2-positive advanced breast cancer. *N Engl J Med.* 2012;367:1783-1791.

22. Barok M, Joensuu H, Isola J. Trastuzumab emtansine: mechanisms of action and drug resistance. *Breast Cancer Res.* 2014;16:209-220.

23. Shefet-Carasso L, Benhar I. Antibody-targeted drugs and drug resistance-challenges and solutions. *Drug Resist Updat.* 2015;*18:36-46.*

24. Kovtun YV, Audette CA, Mayo MF, et al. Antibody-maytansinoid conjugates designed to bypass multidrug resistance. *Cancer Res.* 2010;70:2528-2537.

25. Zhao RY, Wilhelm SD, Audette C, et al. Synthesis and evaluation of hydrophilic linkers for antibody-maytansinoid conjugates. *J Med Chem.* 2011;54:3606-3623.

26. Chen Y. Drug-to-antibody ratio (DAR) by UV/Vis spectroscopy. *Methods Mol Biol.* 2013;1045:267-273.

27. Fasih A, Fonge H, Cai Z, et al. ^{111}In-Bn-DTPA-nimotuzumab with/without modification with nuclear translocation sequence (NLS) peptides: an Auger electron-emitting radioimmunotherapeutic agent for EGFR-positive and trastuzumab (Herceptin)-resistant breast cancer. *Breast Cancer Res Treat.* 2012;135:189-200.

28. Lindmo T, Bunn PA, Jr. Determination of the true immunoreactive fraction of monoclonal antibodies after radiolabeling. *Methods Enzymol.* 1986;121:678-691.

29. Ritter CA, Perez-Torres M, Rinehart C, et al. Human breast cancer cells selected for resistance to trastuzumab in vivo overexpress epidermal growth factor receptor and ErbB ligands and remain dependent on the ErbB receptor network. *Clin Cancer Res.* 2007;13:4909-4919.

30. Erickson HK, Park PU, Widdison WC, et al. Antibody-maytansinoid conjugates are activated in targeted cancer cells by lysosomal degradation and linker-dependent intracellular processing. *Cancer Res.* 2006;66:4426-4433.

31. Sorkin A, Duex JE. Quantitative analysis of endocytosis and turnover of epidermal growth factor (EGF) and EGF receptor. *Curr Protoc Cell Biol.* 2010;Chapter 15:Unit 15 14.

32. Xu S. Internalization, trafficking, intracellular processing and actions of antibody-drug conjugates. *Pharm Res.* 2015;32:3577-3583.

33. Smith LM, Nesterova A, Alley SC, Torgov MY, Carter PJ. Potent cytotoxicity of an auristatin-containing antibody-drug conjugate targeting melanoma cells expressing melanotransferrin/p97. *Mol Cancer Ther.* 2006;5:1474-1482.

34. Law CL, Cerveny CG, Gordon KA, et al. Efficient elimination of B-lineage lymphomas by anti-CD20-auristatin conjugates. *Clin Cancer Res.* 2004;10:7842-7851.

35. Berger C, Madshus IH, Stang E. Cetuximab in combination with anti-human IgG antibodies efficiently down-regulates the EGF receptor by macropinocytosis. *Exp Cell Res.* 2012;318:2578-2591.

36. Veronese FM, Mero A. The impact of PEGylation on biological therapies. *BioDrugs.* 2008;22:315-329.

37. Strop P, Delaria K, Foletti D, et al. Site-specific conjugation improves therapeutic index of antibody drug conjugates with high drug loading. *Nat Biotechnol.* 2015;33:694-696.

38. Xie H, Audette C, Hoffee M, Lambert JM, Blattler WA. Pharmacokinetics and biodistribution of the antitumor immunoconjugate, cantuzumab mertansine (huC242-DM1), and its two components in mice. *J Pharmacol Exp Ther.* 2004;308:1073-1082.

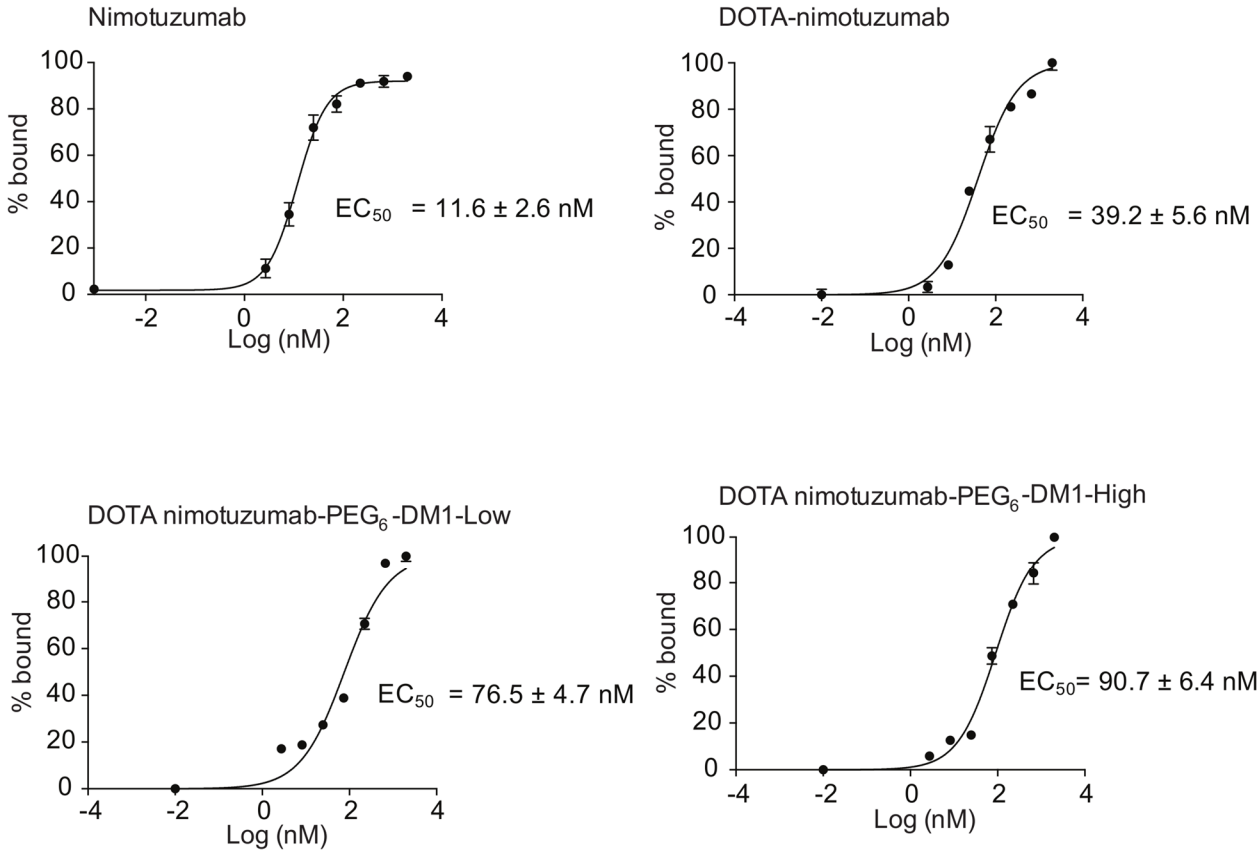

FIGURE 1: *In vitro* flow cytometry binding assay. DLD-1 cells were titrated with nimotuzumab, DOTA-nimotuzumab, DOTA-nimotuzumab-PEG$_6$-DM1-Low and DOTA-nimotuzumab-PEG$_6$-DM1-High and analyzed by flow cytometry.

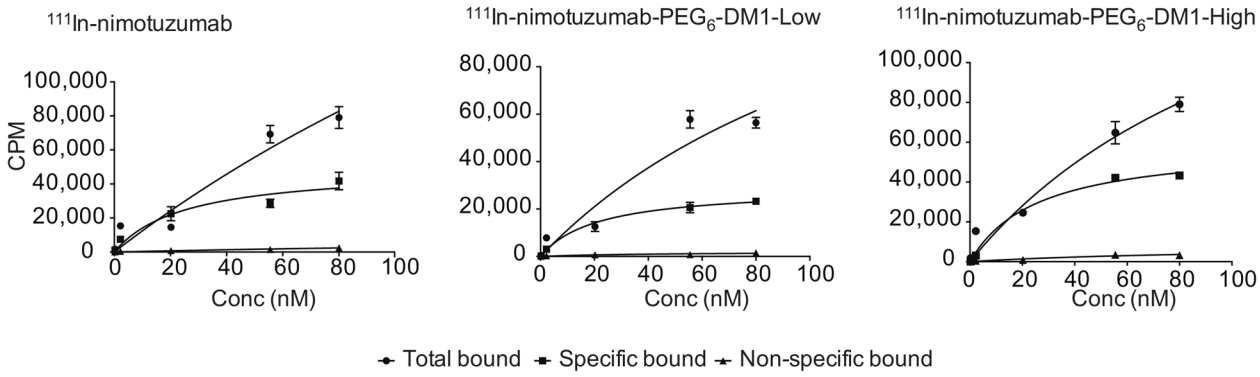

FIGURE 2: Saturation radioligand binding assay. ^{111}In-nimotuzumab, ^{111}In-nimotuzumab-PEG$_6$-DM1-Low and ^{111}In-nimotuzumab-PEG$_6$-DM1-High were tested for binding to EGFR positive DLD-1 cells. CPM = Counts per minute.

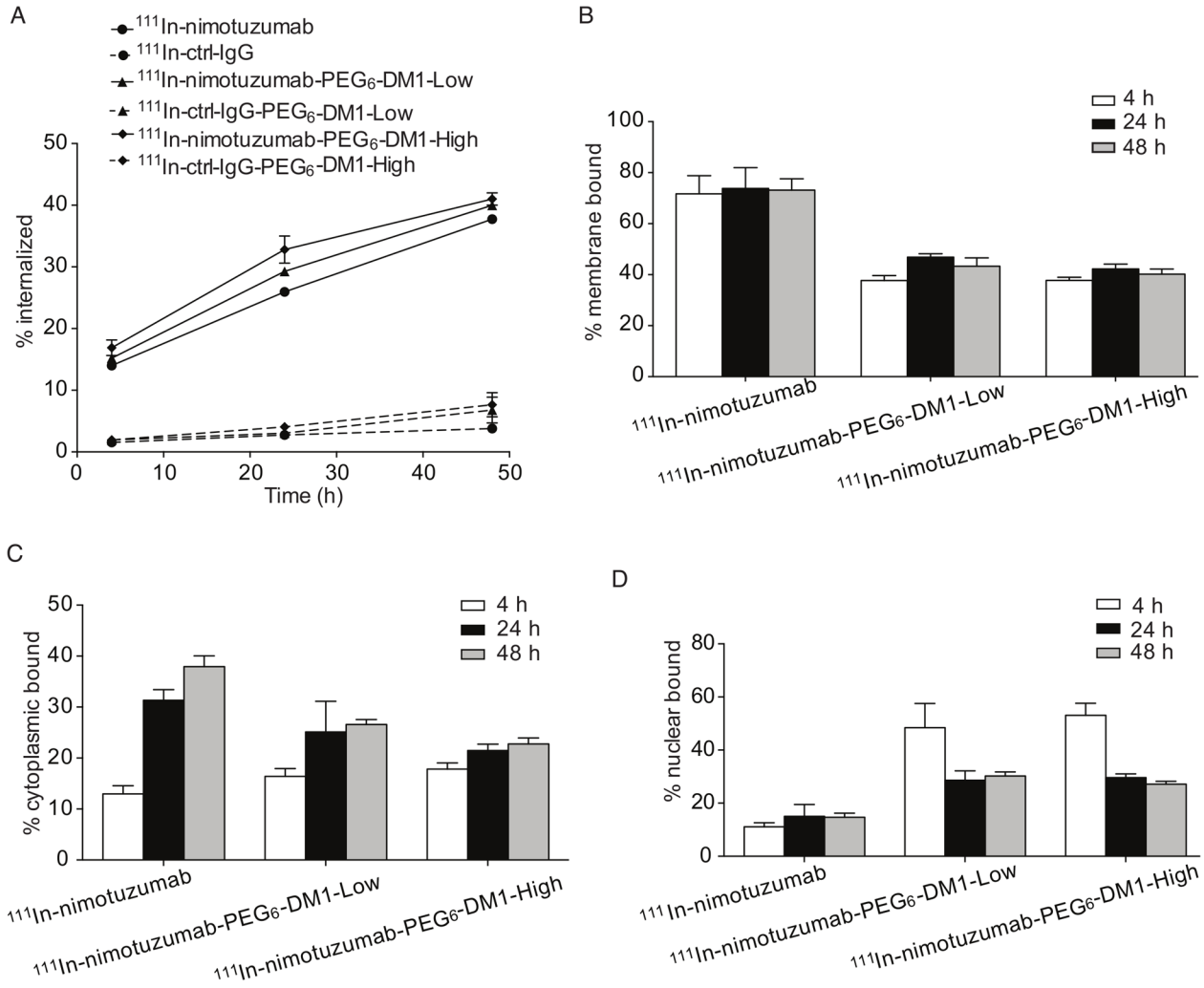

FIGURE 3: EGFR mediated internalization. A) ^{111}In-nimotuzumab, ^{111}In-nimotuzumab-PEG$_6$-DM1-Low, ^{111}In-nimotuzumab-PEG$_6$-DM1-High, control antibody (^{111}In-ctrl-IgG) and control antibody drug conjugates (^{111}In-ctrl-IgG-PEG$_6$-DM1-Low and ^{111}In-ctrl-IgG-PEG$_6$-DM1-High) were tested for EGFR mediated internalization using DLD-1 cells at 4 , 24 and 48 hours (h) post incubation. A) Total internalized radioimmunoconjugate, B) total membrane bound, C) cyctoplasmic bound and D) nuclear uptake.

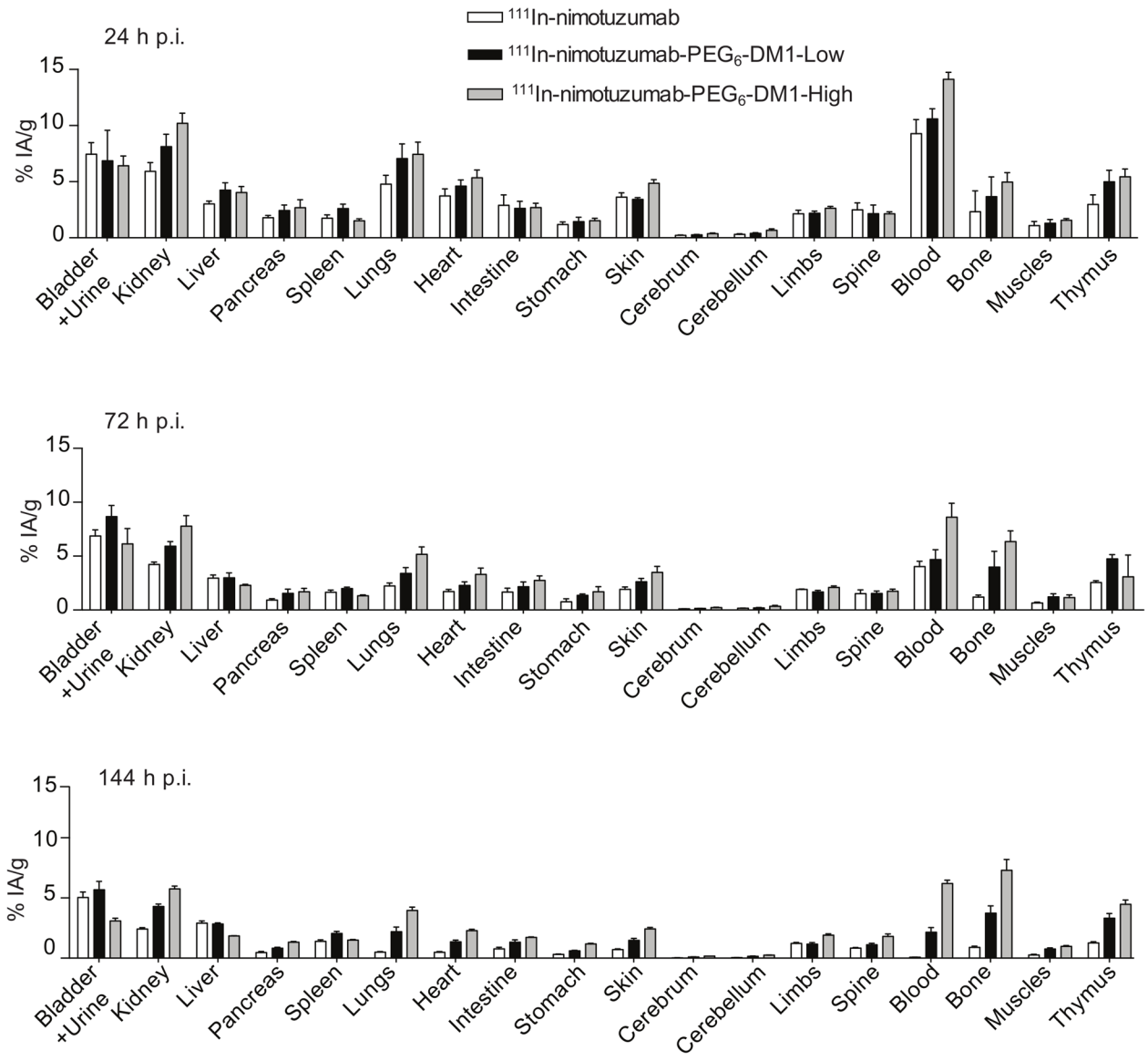

FIGURE 4: Biodistribution in healthy Balb-C mice of ^{111}In-nimotuzumab, ^{111}In-nimotuzumab-PEG$_6$-DM1-Low and ^{111}In-nimotuzumab-PEG$_6$-DM1-High at 24 h p.i., 72 h p.i. and 144 h p.i..

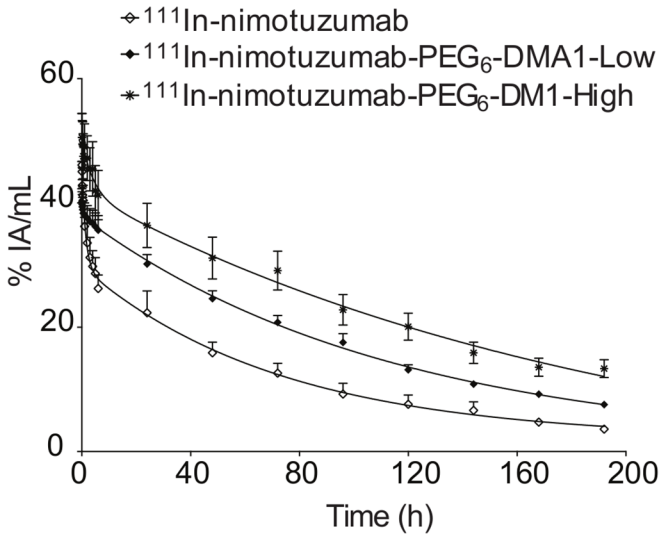

FIGURE 5: Pharmacokinetics of ^{111}In-nimotuzumab, ^{111}In-nimotuzumab-PEG$_6$-DM1-Low, ^{111}In-nimotuzumab-PEG$_6$-DM1-High in healthy Balb/C mice.

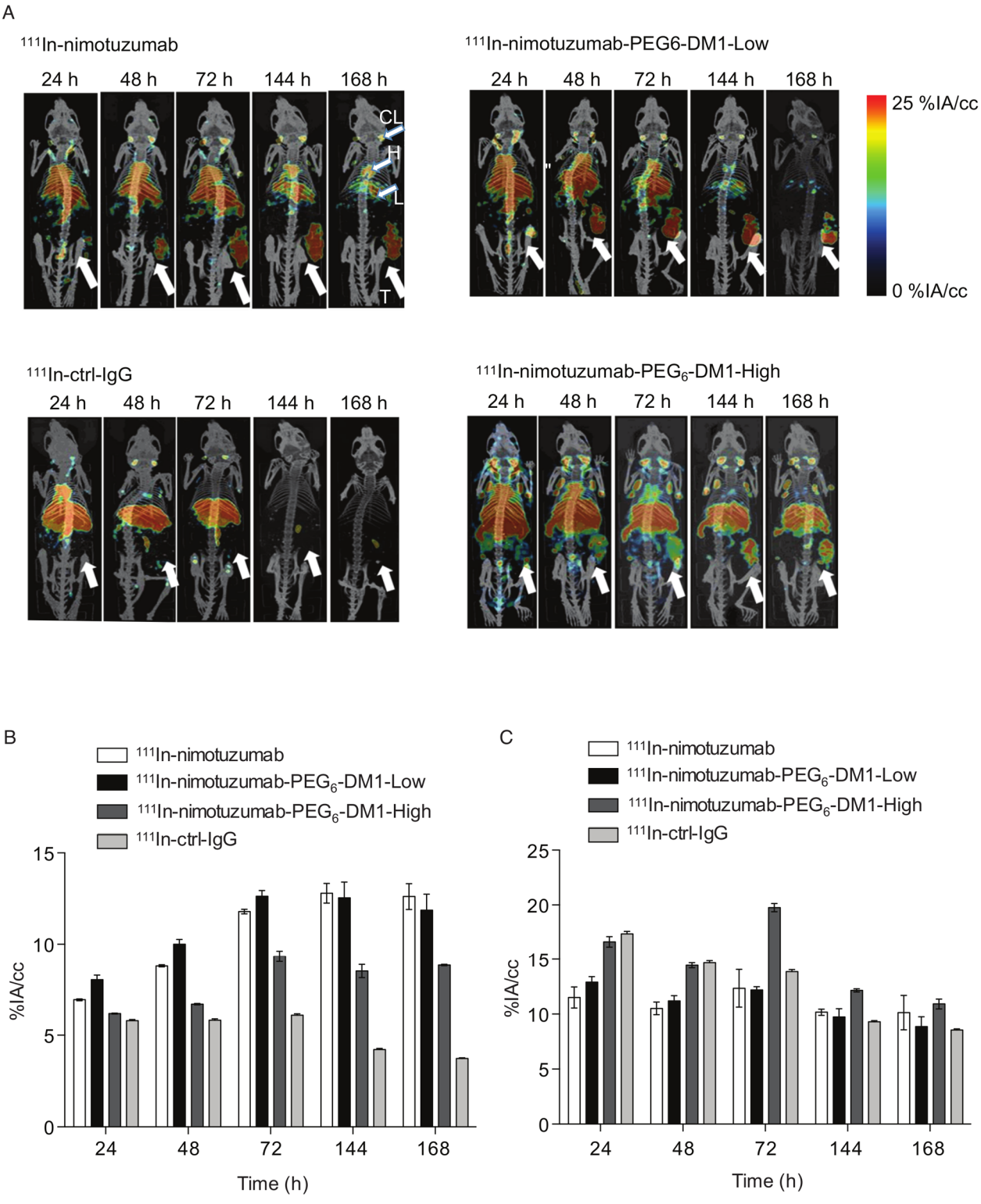

FIGURE 6: A) MicroSPECT/CT imaging. ^{111}In-nimotuzumab, ^{111}In-nimotuzumab-PEG$_6$-DM1-Low, ^{111}In-nimotuzumab-PEG$_6$-DM1-High and control antibody ^{111}In-ctrl-IgG microSPECT/CT

imaging in mice bearing DLD-1 tumors in their right hind leg (white arrow) at 24 h, 48 h, 144 h and 168 hours (h) p.i. (n = 4 per tracer per time point). Where arrow indicate the position of organs, CL: cervical lymph node, H: heart, L: liver, and T: tumour. B) Tumor time activity uptake from microSPECT. C) Liver time activity uptake.

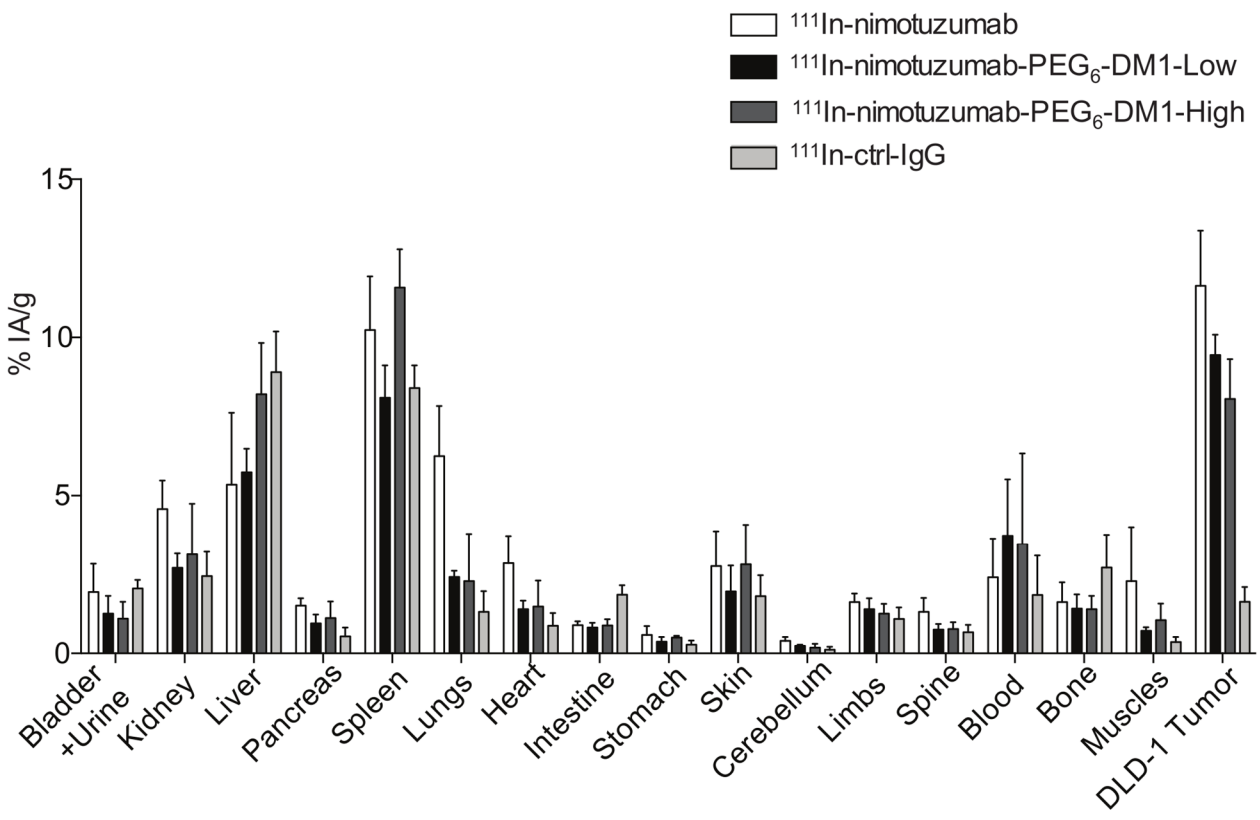

FIGURE 7: Biodistribution of ^{111}In-nimotuzumab, ^{111}In-nimotuzumab-PEG$_6$-DM1-Low, ^{111}In-nimotuzumab-PEG$_6$-DM1-High and control antibody, ^{111}In-ctrl-IgG in athymic CD-1 nude mice bearing DLD-1 tumors at 168 h p.i.

Tables

Table 1: Binding constants (K_D) association constants (K_{on}) and dissociation constants (K_{diss}), by biolayer interferometry of antibody and immunoconjugates

Construct	K_D (nM)	K_{on} (1/Ms)	K_{diss}(1/s)
Nimotuzumab	0.62 ± 0.01	$5.8 \pm 0.02 \times 10^4$	$3.2 \pm 0.06 \times 10^{-5}$
DOTA-nimotuzumab	1.05 ± 0.13	$7.38 \pm 0.02 \times 10^4$	$7.76 \pm 0.05 \times 10^{-5}$
DOTA-nimotuzumab-PEG_6-DM1-Low	3.53 ± 0.04	$6.25 \pm 0.03 \times 10^4$	$1.95 \pm 0.02 \times 10^{-4}$
DOTA-nimotuzumab-PEG_6-DM1-High	13.02 ± 0.01	$3.77 \pm 0.09 \times 10^4$	$4.91 \pm 0.03 \times 10^{-4}$

Table 2: Pharmacokinetic parameters of ^{111}In-nimotuzumab, ^{111}In-nimotuzumab-PEG$_6$-DM1-Low, and ^{111}In-nimotuzumab-PEG$_6$-DM1-High in healthy Balb/C mice. Mean values ± SEM

Construct	Half-life $t_{1/2\alpha}$, (h)	Half-life $t_{1/2\beta}$, (h)	AUC (% IA.hr/mL)	V_{ss} (mL)	CL (mL/hr × 10^{-2})
^{111}In-nimotuzumab	2.3 ± 0.7	165 ± 29.6	1096.8 ± 6.3	19.3 ± 3.9	9.1 ± 1.0
^{111}In-nimotuzumab-PEG$_6$-DM1-Low	17.6 ± 7.3	217.2 ± 24.7	2293.5 ± 299.9	10.9 ± 4.6	5.0 ± 1.0
^{111}In-nimotuzumab-PEG$_6$-DM1-High	4.8 ± 0.1	433.1 ± 0.0	2791.6 ± 140.8	19.9 ± 1.0	4.0 ± 0.2